

Cracking and shape deformation of cylindrical cavities during constrained sintering

Tobias Rasp^a, Christine Jamin^b, Olivier Guillon^c, and Torsten Kraft^{a,1}

^a Fraunhofer Institute for Mechanics of Materials IWM, 79108 Freiburg, Germany

^b Institute of Materials Science, Technische Universität Darmstadt, 64287 Darmstadt, Germany

^c Forschungszentrum Jülich GmbH, Institute of Energy and Climate Research IEK-1: Materials Synthesis and Processing, 52425 Jülich, Germany

¹ Corresponding author

Abstract

During constrained sintering of thin films, in which a cylindrical cavity with axis perpendicular to the substrate has been introduced before sintering, cracks emerge that initiate at the cavity surface. By combining experiments with continuum mechanical and particle based simulations, the fundamental causes and effects of this kind of crack formation are identified. A stress analysis performed by finite element (FEM) simulations matches with the cracking behaviour observed in experiments. A comparison of discrete element (DEM) results with experiments shows the applicability of this simulation method to describe the effect of cross-sectional stripe dimensions and cavity diameters on the cracking behaviour. Moreover, DEM simulations reveal that hair-line cracks in narrow stripe samples formed during pre-sintering manufacturing steps might be a dominant cause for the observed crack damage in such systems.

Keywords: constrained sintering, simulation, thin films, alumina, cracking

1. Introduction

Crack formation during sintering can be a significant problem in many applications of multi-material composites. For example, LTCC components as used in electrical, chemical or microfluidic systems are composed of multi-layered ceramics and metals to build up 3D circuits [1]. During manufacturing of the required thin films, agglomerates of organic material may form that are burnt out before sintering starts. This can lead to the formation of internal voids or flaws at the surface of the film, which may be significantly larger than the particle scale [2]. On the other hand, internal voids can also emerge during co-firing if the layer material is a composite containing powder agglomerates with a higher sintering rate relative to the rate of the surrounding powder matrix [3,4]. Moreover, some voids are also introduced intentionally in the green films as defined cavities that later act as e.g. connection vias between the individual layers in a laminated multi-layer stack. In all of these cases it is important to know how size and shape of those voids develop during sintering and whether these internal surfaces are critical for crack formation and, consequently, turn out to be origins of functionality failure.

Only few experimental studies investigated systematically the problem of crack initiation and development at such internal surfaces by introducing pre-defined, artificial defects before constrained sintering. Bordia et al. [5] analysed the damage and fracturing behaviour in constrained sintered glass and alumina films of different thicknesses containing pre-existing, crack-like defects. They observed that crack growth occurs above a critical film thickness for the case of the glass film. The alumina film, however, just showed a diffuse damage zone ahead of the crack tip, so no conclusions could be drawn for the crack growth in the alumina films. Cracks have also been observed by Green et al. [4], who presented in their review article an image of a circular via through a ceramic thin film after sintering showing obvious damage in form of cracks that are oriented radially around the void. However, this behaviour neither was explained nor discussed in detail in this work. With the goal of optimizing the functionality of solid oxide fuel

cells, Wang et al. [6] studied the defect evolution during constrained sintering of thin films composed of two different ceramic electrolyte materials. After binder burn-out they introduced artificial cracks in the films by Vickers indentation and observed a remarkable crack opening in the subsequent sintering step. Since no cracks at all appeared in the constrained sintered film when no artificial defects have been introduced before, they concluded that the existence of defects in the pre-sintering state is a necessary condition for cracking.

The problem of crack formation at pre-existing defects during constrained sintering was also investigated numerically in the past. Applying the so-called material point method, which uses a local empirical failure criterion and is based on continuum mechanical methods, Li et al. [7] simulated a simple system of a film with a rectangular defect. As a main result it was observed that all cracks develop at the corners, where the curvature of the defect is maximum. The first discrete element method (DEM) study about crack initiation during sintering was published by Henrich et al. [8], where a film composed of particles was constrained in one lateral direction and a notch has been introduced at the free film edge acting as a crack propagation seed. Providing that particle rearrangement was hindered by high inter-particle friction, a crack formed ahead of the notch tip and propagated through the whole sample in their simulations.

The fact of inter-particle friction playing a crucial role for crack formation was further pointed out by Martin et al. [9]. Here, sintering of a thin film was simulated by DEM. The film was constrained by two opposing substrates in width direction, while free boundaries were used in thickness and the second width direction. Additionally, a crack-like defect was included in the system as an extra free surface, which passes through the whole film thickness and is situated in the interior of the film similar to the one in the experimental study of Bordia et al. [5] mentioned above. Applying a high friction coefficient, the pre-existing defect grows and new cracks form with direction perpendicular to the free edge. In contrast, sintering with a friction coefficient value of zero did not lead to an effect on the initial crack at all. However, severe cracking behaviour was

also observed in samples that did not contain a pre-existing defect when inter-particle friction was high. On the other hand, sintering samples that contain a predefined defect but were not constrained in lateral direction lead to a closure of the defect. Therefore, these authors concluded that the geometrical constrained is a necessary condition for crack formation, but the existence of a predefined defect as a cracking seed is not in their case.

In contrast to the studies above, the intentionally introduced voids in the thin film samples regarded in this work are not crack-like or of an edge notch type but cylindrical cavities with major axis perpendicular to the rigid substrate that acts as sintering constraint. The samples are therefore similar to ceramic layers with inserted vias as they are used e.g. in ceramic multi-layer stacks for electrical and chemical applications. Due to the progressing miniaturization of mechanical, optical and electronic devices, a profound understanding about edge effects arising during manufacturing is inevitable. Therefore, not only films with approximately infinite width (continuous films), but also with finite lateral dimensions (stripe samples) had been investigated.

In this study, two different simulation approaches were employed besides an experimental investigation to analyse the cracking behaviour in the vicinity of a cavity. The finite element method (FEM) based on continuum mechanics is the preferred method for calculating accurate stress distributions in short simulation times. In recent years, it has been successfully applied especially for the prediction of shape deformations during sintering [10,11]. However, the simulation of crack propagation is complicated with this method requiring either complex remeshing and element deletion procedures of the geometry or the use of advanced – and sometimes controversial – methods like XFEM (extended finite element method). Moreover, the continuum mechanical approach using FEM requires the application of a phenomenological damage initiation criterion. In our study, therefore, FEM has mainly been employed only for predicting the local stresses around cavities as well as geometrical changes of the cavity shapes, whereas the actual crack formation and propagation has been simulated by the particle-

based DEM. Here, each grain of the ceramic powder is considered as a distinct particle that is able to move freely under conditions of interactions with neighbouring grains. As a consequence, this method is much more computation time consuming but the effect of crack initiation is included by design.

In the following, the applied simulation methods and the experimental procedure for solid state sintering of thin films on a rigid substrate are introduced. Results for all of the three different methods are contrasted with each other with a focus on the cracking behaviour at the cavity for stripes with variable geometry. Finally, the findings are discussed with regard to the origin of the observed effects and to discrepancies between the outcomes of the different methods.

2. Experiment and simulation description

Preparing appropriate green stripe samples with predefined cavities for sintering experiments and simulations is a challenging task. While the manufacturing of micro-sized and standalone samples with high aspect ratios on a substrate requires sophisticated and elaborate experimental methods like soft lithography, the difficulty of initial sample design for simulations is mainly about finding an appropriate choice of boundary conditions and a suitable dimensioning of the sample in order to keep the computational costs within a reasonable limit. Examples of green samples for the individual methods employed in this study are shown in Fig. 1. Manufacturing details and modelling concepts will be described in detail in the following subsections.

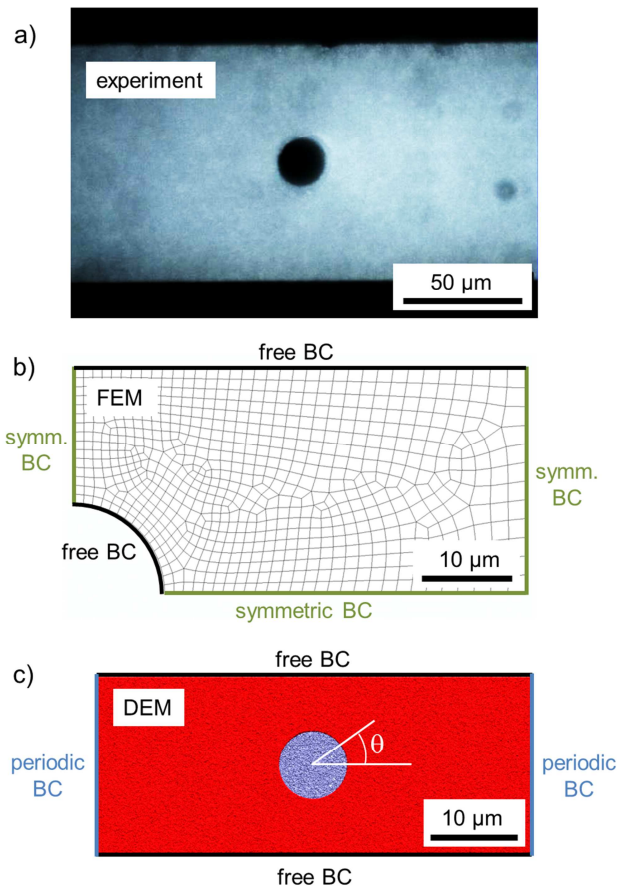


Figure 1: Top view on examples of green stripes on a rigid substrate including a cylindrical cavity in experiment (a) and as used for FEM (b) and DEM calculations (c). The DEM sample consists of 2.35 Mio. particles (red particles represent the film, blue particles represent spatially fixed substrate particles).

2.1. Experimental procedure

The experimental procedure to generate clearly separated stripe samples with high aspect ratio on a smooth substrate by micro-moulding in capillaries (MIMIC) is described in detail by Guillon et al. [12,13]. In this study, an aqueous slurry made of 50 vol% alumina powder with an average particle size of $d_{50} = 150$ nm (TM-DAR, Taimei Chemical, Tokyo, Japan) dispersed in deionized

water was used. The high solid loading was chosen to minimize drying shrinkage and stresses that may lead to cracking around cavities in the green samples. Stripes with different thicknesses and widths were produced containing cavities with varying diameter. For this purpose, a PDMS (polydimethylsiloxane) stamp was produced as a forming tool for the stripe structures [13]. In order to create the cavities during the MIMIC procedure, the channels in the stamp contain placeholders that later-on leave behind the desired gaps in the stripes when the slurry fills the capillaries of the stamp [13]. An example of a dried green stripe with cavity as used in the experiments is shown in Fig. 1a.

The samples were sintered on a sapphire substrate at 1450 °C for 4 h using a heating rate of 25 °C/min up to 1200 °C followed by 10 °C/min up to 1450 °C. The cylindrical cavities were analysed using scanning electron microscopy (Philips XL3000 FEG, FEI Company, Eindhoven, Netherlands) top view pictures of the stripes at the end of the isothermal holding time. Moreover, in-situ environmental scanning electron microscopy (ESEM, Quanta 200F, FEI Company, Eindhoven, Netherlands) experiments were performed to analyse the crack propagation at the cavities during sintering. The as-deposited films were heated up to 1000 °C for 15 min to provide some mechanical stability. This stability is required for the subsequent dry cutting of the specimens using a diamond wire saw without any measurable densification. The sintering schedule deviates from the one used in the ex-situ experiments. The heating rate was lowered progressively with increasing temperature in order to guarantee a high image quality and a maximum temperature of 1300 °C was chosen for all specimens.

2.2. FEM simulation method

Finite element (FEM) simulations have been performed to compute magnitude and location of stresses that arise around the cylindrical cavities during constrained sintering. The solid state sintering model applied for this purpose goes back to the approach of Riedel et al. [14,15]. This

model is based on the classical concepts of sintering, where the driving force for sintering is the minimization of the internal surface energy. It takes diffusive transport of matter by grain boundary, surface and volume diffusion as well as rearrangement and grain coarsening into account, and distinguishes between open and closed porosity. Since this transition is continuous, a numerical interpolation is applied. The constitutive equation is expressed as a linear relation between the macroscopic strain rate tensor and the stress tensor. The latest version of the sintering law used for the calculations is summarized in previous publications [10,11], which have been implemented as a user subroutine in the commercial FE software Abaqus in order to simulate sintering on a rigid substrate.

All calculations had been performed in 3D using Abaqus/Standard with finite elements of type C3D8I and sizes ranging from 0.2 μm to 2.0 μm by simulating a quarter of the stripe sample and applying symmetric boundary conditions in longitudinal stripe directions and at the inner part of the sample in lateral direction (see Fig. 1b). The outer part in lateral direction and the upper surface of the stripe have free boundaries. The final 3D mesh is created by extruding the unstructured 2D mesh shown in Fig. 1b in thickness direction. Using an automatically created unstructured 2D mesh in the in-plane direction is permissible if the individual deviations of the edge angles are in a reasonable range. In contrast to regular meshes such unstructured meshes often benefit of better element aspect ratios.

The lower surface of the sample is constrained by a rigid substrate. The interaction between substrate and film has been modelled using the Abaqus methods *coulomb friction* and *damage initiation* assuming that both surfaces stay together (using *cohesive behavior* in Abaqus) as long as there is no crack initiation. The damage initiation criterion used is based on the maximum nominal stress criterion. Apparently, the length of the delamination cracks that typically occur at the substrate interface when thin films are sintered on rigid substrates [16] are mainly determined by the value of the maximum nominal stress in the normal-only mode. The critical

normal stress was determined to be 0.95 MPa in a former study [13], since simulations with this value showed a good match with experimental measurements concerning delamination crack length.

As explained above, the focus of the FEM analysis of this study is only on investigating stress formation at cavities. Therefore, damage initiation was disabled in the body of the film, i.e. no stress relief by cracking was allowed to occur in the interior of the film although the maximum nominal stress might exceed the critical value found for the interaction between substrate and film. Moreover, since determining precise model parameters for a new material is quite time demanding including special experiments only qualitative conclusions about stress development computed by FEM are aimed at. Therefore, an existing parameter set related to zirconia toughened alumina (ZTA) [11] has been used for the FEM calculations. This choice can be justified since ZTA usually has only a few vol% zirconia added to the alumina matrix so that the relevant prevailing sintering mechanisms should be comparable to the alumina used in the DEM simulations and experiments of this study.

2.3. DEM simulation method

The DEM is a simulation method for which each grain is regarded as a distinct particle that interacts with neighbouring particles by given force laws. All particles are defined by their positions and radii and are considered to be free in translational and rotational motion. Therefore, processes taking place on the particle scale like particle rearrangement and crack initiation are included in the method by design and can easily be monitored. In the context of DEM, a defect can form and propagate as soon as a set of particles moves as a group in an opposing direction relative to neighbouring particles due to inhomogeneous sintering conditions. This leads to collective particle contact rupture leaving behind voids in the structure. Here, a

defect is seen as a crack if its width is above one particle diameter and its longitudinal extension is considerably larger than its width [8, 9].

The force laws defining the particle-particle interaction in the DEM framework used in this study have been chosen as in the studies of Henrich and Wonisch [8,17] and are – similarly to the FEM model introduced in the last section – based on the sintering model by Riedel and Svoboda [14,15]. Since a detailed definition of the applied simulation procedure can be found in previous publications [8,18], only a short description of the model is given here. The model assumes that grain boundary diffusion is the main transport mechanism for sintering, the surface of the pores is in equilibrium and neighbouring contacts do not interact. This is valid for the state of open porosity presuming a (infinitely) fast surface diffusion. As a consequence, the DEM sintering simulations provide reasonable results just up to a relative density of about 90%. Taking these conditions into account, the interaction between two particles in contact can be described by a normal force, which is split into an attractive sinter force and an opposing repulsive viscous force, and a tangential force, which represents a viscous resistance against sliding (thus also referred to as interparticle friction) [8]. Here, the viscous forces rise quickly with increasing neck radius between two contacting particles leading to diminishing particle-particle approach and sliding. The total force as well as the total torque acting on one particle is calculated from the sum of particle–particle forces and torques. The temporal evolution of the particle system is governed by Newton’s equations of motion.

The material parameters presented in a preceding publication [16] had been adapted to the TM-DAR alumina powder, i.e. the same powder that was now used in the experiments of the current study. Therefore, all DEM simulation parameters defining the forces were taken from [16]. This includes the choice of particle size, particle size distribution, the tangential grain boundary viscosity coefficient, the activation energy for grain boundary diffusion and the material data of alumina. In contrast to the former study, the relative green density was set to an uniform value of

57% for all samples for a better comparability of the results. The starting temperature was set to 1200 °C to avoid disproportionately small time steps, which occur at low temperatures, assuming that no significant sintering activity takes place below this temperature. In order to reduce very long simulation times in the DEM simulations, a heating rate of 25 K/min was applied to the samples until a hold temperature of 1450 °C has been reached. This is different from the experiments, where a heating rate of 10 K/min has been applied in this temperature range. However, comparing the DEM results concerning local density distribution und crack formation of a reference sample calculated with both heating rates revealed only slight differences. On the other hand, the calculation time increased by a factor of 2 when applying the experimental heating rate. This is due to high viscous forces at low temperatures that require very small time steps over a longer period until high temperatures are reached. Consequently, the higher heating rate was used for all calculations assuming that this argumentation holds also in other cases.

Initial particle configuration generation for the DEM simulations was performed as described in a previous publication [16]. This means in particular that the particle size distribution parameters and cross-sectional dimensions were adapted to data from the accompanying experiments. Moreover, the rigid substrate was represented also by particles that are spatially fixed during the simulation. In the case of a film particle being in contact with a substrate particle, the normal force between these particles F_{sp}^n is related to the normal force between two film particles F_{pp}^n by $F_{sp}^n = 0.64 F_{pp}^n$. The factor 0.64 is the outcome of fitting simulation results to experimental measurements in a former study [19], where stripe edge delamination values were recorded during sintering of thin stripes on a substrate with equal configuration as in this study for both simulations and experiments. Therefore, the relation above holds also for the tests in this study but is presumably not universally valid. The cylindrical cavity was created by simply removing all particles from the corresponding region of the stripe.

In the length direction of the samples, fixed periodic boundary conditions were applied, i.e. particles leaving the simulation box on a periodic boundary are translated to the opposite boundary and particles within a certain interaction radius to a periodic boundary can interact with particles at the opposite boundary. Thus, this condition on the one hand causes the sample to behave like an infinitely long stripe by replicating the simulation cell in longitudinal direction. This reflects the stripe nature of the real experimental sample, where the length dimension is some magnitudes larger than the cross-sectional dimensions. On the other hand, the periodic boundaries prohibit any shrinkage of the sample in length direction since they are fixed. This induces tensile stresses in longitudinal direction, which can be justified by the fact that the substrate acts as a very strong constraint in this direction. Therefore, longitudinal shrinkage occurs only at the respective stripe edges, which are not of interest in this study. Indeed, experiments and simulations showed that lateral shrinkage distant to edges is negligible for stripes sintering on a substrate [16,19].

In order to guarantee that no unwanted interaction effects between cavities occur over the periodic boundaries, the distance between the opposing boundaries had to be chosen fairly large. Preliminary studies showed that a distance of 6.25 times the cavity diameter is a good compromise between reasonable computing times and an appropriate representation of the real stripe geometry [20]. Nevertheless, a rather huge number of particles had to be simulated as expressed for the green DEM sample shown in Fig. 1c.

Consequently, it was no longer possible to simulate a stripe sample with the same cross-sectional dimensions as in the accompanying experiments like it was done in previous DEM sintering studies [13,16,19]. In contrast, all stripe dimensions have been uniformly scaled down compared to the real sample sizes. Stripes with a very large width have been represented by applying periodic boundary conditions also in lateral direction, i.e. mimicking a continuous thin film with cavities. For stripes without cavities and varying sizes, an extensive study has shown

that the sintering behaviour is dominated by the thickness-to-width aspect ratio ξ and not by the sample size itself [10]. Fig. 2 shows exemplarily the evolution of average relative density and the distribution of local relative density in the cross-section for stripes with different cross-sectional dimensions but equal ξ . It is evident that the sintering behaviour is determined by the aspect ratio and is independent of a length scaling factor as samples with similar ξ show similar features. This is in particular true for length and angle of edge delamination cracks at the substrate interface of the samples illustrated in Fig. 2b. Consequently, a downscaling of the system size is permissible without loss of information as long as the system size is by far larger than the entity size (i.e. the particle size in the case of particle simulations), which is fulfilled for the samples used in this study.

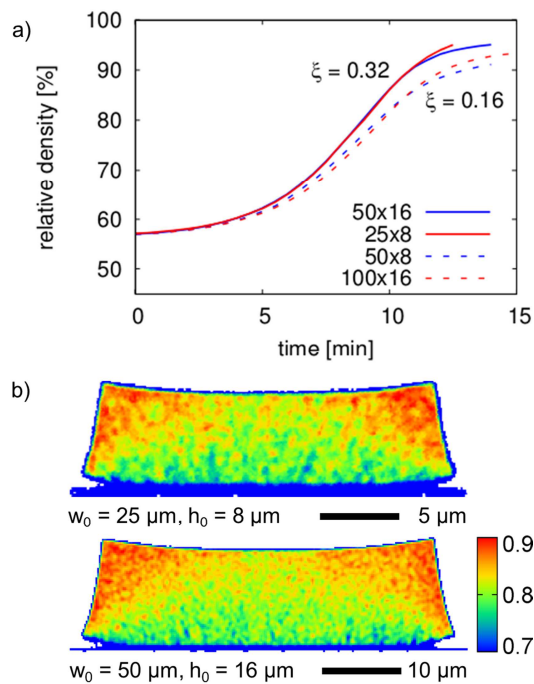


Figure 2: a) Evolution of average relative density in samples with two different aspect ratios ξ and different absolute dimensions (denomination of individual stripes by initial width w_0 x initial height h_0). b) Local relative density distribution in the cross-section of stripes for an aspect ratio $\xi = 0.32$ and two different dimensions sintered up to 80% average density.

2.4. Sample overview

Stripe samples with varying cross-sectional dimensions and cavity diameters have been experimentally manufactured and generated as simulation input in order to evaluate the influence of those parameters on the cracking behaviour around cavities during constrained sintering. An overview of the complete set of samples investigated in this study for the three individual methods is given in Tab. 1 including the respective width W and thickness H of the stripe cross-sections as well as the cavity diameter D . All values refer to the green state of the samples. In the case of DEM, the width W of the sample with periodic boundary conditions applied in both lateral directions (sample DEM2) is specified as ∞ indicating that this sample represents a continuous, infinitely wide film. In the following, the denomination of a particular sample is according to short name of the method together with the sample number.

Sample No.	Experiment			FEM			DEM		
	H	W	D	H	W	D	H	W	D
	[μm]								
1	16	50	20	25	50	20	10	20	8
2	16	250	20	25	500	20	10	∞	8
3	11	50	20	10	50	20	6	20	8
4	27	50	20	50	50	20	20	20	8
5	27	100	10	25	500	10	10	20	4
6	27	100	50	25	500	50	10	20	12

Table 1: Cross-section thickness H and width W in the green state of all stripe samples investigated in this study together with the diameter D of the cylindrical cavities within the samples.

3. Influence of stripe and cavity dimensions

3.1. General stress distribution and cavity deformation

Assuming free sintering of stripe samples with internal cavities without a substrate acting as constraint, a uniform and stress-free shrinkage of the samples can be expected where the cavity contracts accordingly in a homogeneous manner. Due to the presence of the substrate in the case of constrained sintering, however, tensile stresses arise in the substrate plane and in longitudinal direction leading to a complex stress distribution around the cavity, which acts as a stress concentrator.

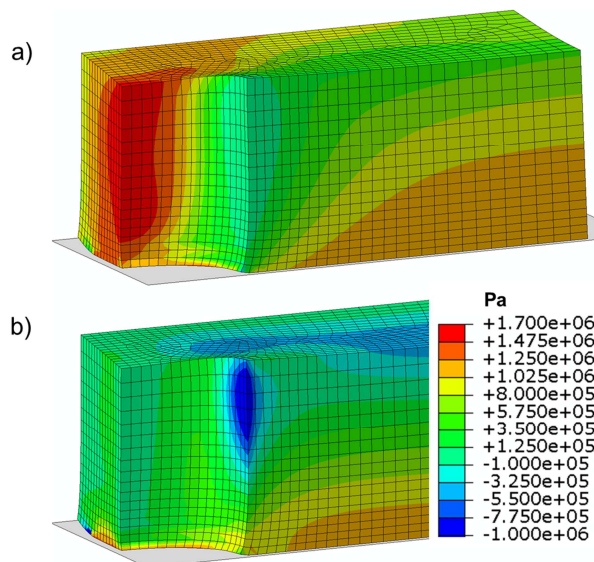


Figure 3: Stresses in longitudinal (a) and lateral (b) stripe directions computed by FEM for the FEM1 sample of Tab. 1.

Fig. 3 shows the stresses in longitudinal and lateral stripe directions computed by FEM for the sintered FEM1 sample of Tab. 1. The stress distributions reveal that the sample experiences a high tensile load in the part between cavity and lateral stripe edge, which is oriented in length direction and decreases with increasing distance from the cavity rim. Contrarily, compressive stresses in lateral direction can be found at the part of the cavity surface that points to the

longitudinal direction promoting densification in this local area. Additionally, bi-axial tensile stresses occur in the vicinity of the substrate that are, however, not caused by the presence of the cavity and are therefore not supposed to be investigated in this study but have been analysed elsewhere [19,20]. Besides the well-known effects of substrate delamination and cross-sectional shape distortion that are typical for thin film sintering on a substrate [13,16], this stress distribution on the one hand indicates an increased probability for the initiation of cracks starting at the cavity rim and being directed to the lateral edge. On the other hand, since the cylindrical cavity represents a free boundary of the sample, the tensile load has the ability to deform the cavity shape or increase its size depending on the system constraints. In the example of the narrow FEM1 stripe shown in Fig. 3, it apparently leads to an elliptical deformation of the originally circular cavity.

3.2. Variation of stripe width

Stripes with constant thicknesses and cavity diameters but different lateral widths were sintered on a substrate experimentally as well as in FEM and DEM simulations. The individual width increase factors from samples on the left-hand side to samples on the right-hand side are given above the arrows in Fig. 4. Instead of visualising stress distributions for single directions as in Fig. 3, the maximum principal stresses in the samples, which describe the potential areas of cracking more clearly, are visualized as FEM results here. The complex stress distribution calculated by FEM (see Fig. 4a and b) is reflected in the DEM results given also in Fig. 4. First, the elliptical deformation of the originally circular cavity in the narrow stripe can be likewise observed in the DEM result in Fig. 4c. Additionally, a region between the cavity and the lateral stripe edge contains a number of cracks and pores, which start at the cavity and are directed mainly to the lateral edge (oriented cracking) as a consequence of the tensile stresses acting there. In principle, the same behaviour can also be found in the experiments as Fig. 4e shows

for the narrow Exp1 stripe. In contrast to the DEM result, however, one single well-defined crack has been developed besides several smaller cracks. The phenomenon of oriented cracking resembles the DEM results of Henrich et al. [8] and Martin et al. [9], who found that defect opening occurs in the constrained direction while cracking develops perpendicular to the free edge in pre-notched samples constrained by two opposing rigid plates.

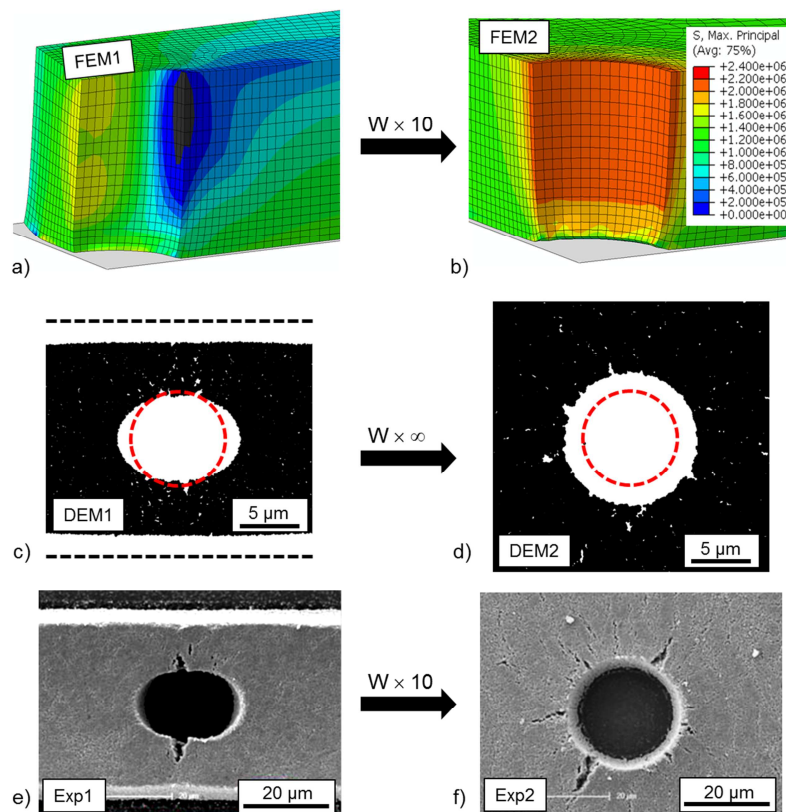


Figure 4: Maximum principal stresses computed by FEM (top), crack and pore development simulated by DEM (centre) and SEM top view images from experiments (bottom) at the cavity region of stripes with different lateral widths sintered on a rigid substrate. The black dashed lines in c) indicate the original stripe edge locations in the green state, the red dashed circle in c) and d) marks the original cavity size. The factor ∞ for the DEM comparison (c and d) expresses the fact that the wider stripe is modelled by applying periodic boundary conditions in both lateral directions mimicking a continuous thin film.

In the case of sintering a wide stripe on a substrate, Fig. 4b shows that high tensile stresses arise all around the cavity. This is reflected in the DEM results by the formation of cracks that start at the cavity rim and are directed to the cavity centre (radial cracking, see Fig. 4d). This behaviour is in good agreement with the experimental observation of cracking around metal vias in ceramic dielectrics as shown by Green et al. [4]. Moreover, one of the cases in the DEM study of Martin et al. [9] indicated such cracking behaviour, where the originally slit shaped defect becomes rounded in the final stage of sintering and small cracks appeared with orientation normal to the defect rim. The cavity in the DEM2 stripe shown in Fig. 4d is no longer elliptically deformed but has expanded uniformly in each direction, i.e. increasing the diameter but retaining the circular shape. Both effects, radial cracking and uniform cavity expansion, are generally in very good accordance with the experimental finding shown in Fig. 4f, where the cracks are slightly more pronounced compared to the DEM result.

3.3. Variation of stripe thickness

Comparing the stress distribution of stripes with varying thickness reveals fairly low tensile stresses in the thinner stripe (Fig. 5a), while higher stresses occur in the thicker stripe (Fig. 5b) at the zone between cavity and lateral edge. This is reflected in the DEM simulations and the experiments by a significantly higher tendency to form cracks. Both in the DEM simulations and in the experiments the cracks are oriented to the stripe edge (see Figs. 5d and f), but the Exp4 sample in Fig. 5f has one large crack that caused a complete rupture of the stripe, whereas oriented multi-cracking occurs in the DEM result in Fig. 5d. In contrast, the thin samples DEM3 and Exp3 show almost no cracking at all (Figs. 5c and e).

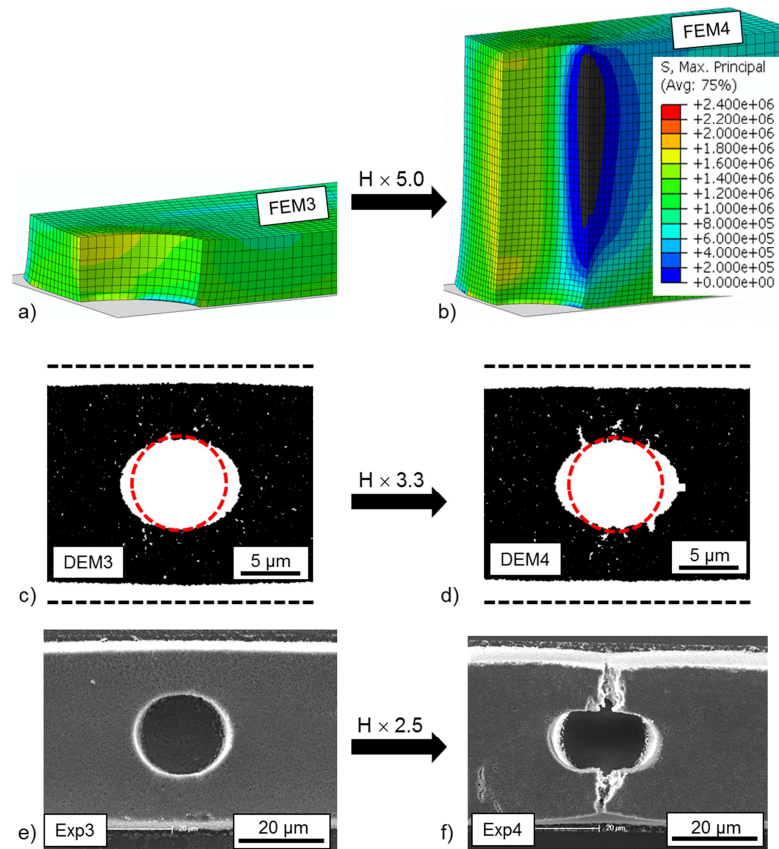


Figure 5: Maximum principal stresses computed by FEM (top), crack and pore development simulated by DEM (centre) and SEM top view images from experiments (bottom) at the cavity region of stripes with different thicknesses sintered on a rigid substrate.

3.4. Variation of cavity diameter

As a last criterion, the diameter of the cavity was varied. For a stripe with small cavity, Fig. 6a shows very high tensile stresses all around the cavity surface that cause increased formation of cracks in both the DEM simulation and the experiment (Figs. 6c and d). In the case of a stripe with large cavity, the stresses are decreased leading to a reduced cracking activity as can be seen from Figs. 6b, d and f. It is remarkable that no cracking occurs in the stripe with the large cavity although in this case the distance between void and stripe edge is much shorter compared to the case of the stripe with a small cavity. This proves that the higher cracking activity in Figs. 6c and e is not an edge effect but caused by the cavity itself. This fact is

supported by the stress images in Figs. 6a and b, where the lateral edge is far away in both cases.

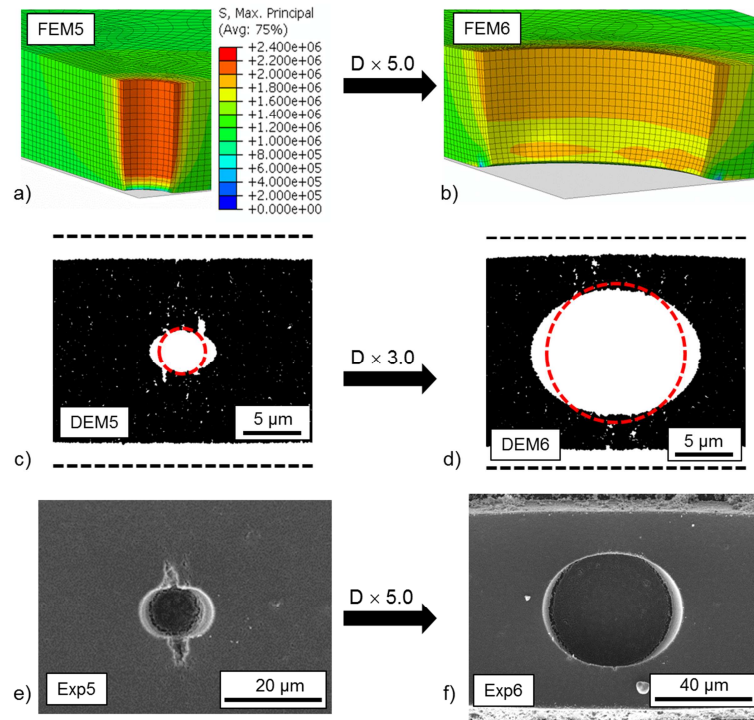


Figure 6: Maximum principal stresses computed by FEM (top), crack and pore development simulated by DEM (centre) and SEM top view images from experiments (bottom) at the cavity region of stripes with different cavity diameters sintered on a rigid substrate.

4. Discussion on crack origin and modelling assumptions

4.1. Origin of stresses and cracks

The results presented in the last section showed that cracking at the cavity can occur in different patterns that depend on the stripe geometry and cavity diameter. The corresponding tensile stresses found in the stripes are in accordance with the classical fracture mechanics theory.

Due to the fact that shrinkage in longitudinal direction is almost completely hindered as a direct effect of the presence of the rigid substrate, the direction of the major internal tensile force is along the stripes main axis. The cavity then acts as a stress concentrator, causing high tensile stresses in the zones between cavity and stripe edges and low stresses in the zones at the cavity that point in longitudinal direction. This behaviour is in principle in accordance with the theoretical prediction for an angular stress dependence $\sigma(\theta)$ at the rim of a perfectly cylindrical cavity $\sigma(\theta) = \sigma_{\infty}(1 - 2 \cos 2\theta)$ [21], where θ is the deviation angle from the stress application axis (see Fig. 1c) and σ_{∞} is a uniform stress applied normal to the cylinder axis, which corresponds to the external stresses induced by the fixed boundary conditions in longitudinal direction in the DEM and FEM case. This relationship shows that the stress around the cavity is minimal (and compressive) in direction of the applied external stress ($\theta = 0^\circ$) and maximal normal to that direction ($\theta = 90^\circ$), which corresponds to the results found in Fig. 3. The stress field developing in the stripes during constrained sintering is, however, generally much more complex than for this simple theoretical thought due the deformation of the stripe during sintering. Therefore, this relationship cannot be transferred one-to-one to the situation investigated in this study.

During sintering of very wide stripes (see Figs. 4b, d and f), high tensile forces not only arise along the main axis of the stripes, but additionally in lateral direction. This is due to lateral shrinkage only occurring in a certain zone parallel to the stripe edge. In the major central part that is far from the lateral edge shrinkage is impeded by the substrate leading to biaxial tensile stresses at the location of the cavity [13,16]. Consequently, high stresses and cracks develop all around the stress concentrator, which are no longer oriented and, therefore, lead to the results shown in Figs. 4d and f.

According to linear elastic fracture mechanics, layer thickness is known to influence the cracking behaviour of continuous films, which are – like the samples regarded in this work – subjected to

biaxial stresses. Former studies [5,22] already identified that there exists a critical film thickness below which no cracking occurs. This is in accordance with the stress fields and cracks presented in Fig. 5, where the thick stripe shows increased tensile stresses and consequently a higher probability for crack formation compared to the thin stripe.

Finally, a decrease of the cavity diameter correlates with a decrease of void curvature and, therefore, with an increase of the stress concentration factor [23]. This leads consequently to higher stresses around the cavities with small diameter in Fig. 6a, which finally results in a higher probability for crack formation at the cavity surface as Figs. 6c and e show.

4.2. Causes for differences in DEM and experiments

The comparison of DEM results and SEM images in section 3 revealed that cracks are somewhat more distinctive in experiment than in particle simulations. For example, the DEM4 stripe in Fig. 5d only includes minor oriented cracks, whereas the corresponding stripe from experiments in Fig. 5f is completely ruptured at the critical location.

One possible reason for this discrepancy might be the occurrence of an unrealistically enhanced particle rearrangement activity in the DEM simulations. The fact of particle friction being a crucial parameter for crack formation has already been reported by other authors as this parameter has a strong influence on the ability of particles to rearrange [8,9]. The key parameter defining the relative sliding behaviour of two particles is the so called tangential viscosity coefficient η , which is a phenomenological parameter and part of the tangential force law as described by Henrich and Wonisch [8,18]. Herein, we use the dimensionless description given by Martin et al. [9]. In all DEM simulations of this study a value of $\eta = 0.027$ was used, which has been adapted to literature values [18]. However, this parameter is generally very hard to determine exactly from

experiments, for which reason it is common to choose a value of a reasonable dimension [24,25] or apply a certain range of values in DEM simulations instead [9,26].

Assuming that the value of this parameter had been chosen too low in the preceding simulations, further simulations have been performed with an increased tangential viscosity coefficient of $\eta = 0.25$. The corresponding results in Fig. 7 show that the cracks formed during constrained sintering are more pronounced compared to the former ones and, therefore, are in a somewhat better accordance to the real cracking behaviour. The narrow stripe in Fig. 7a now features the expected rupture cracks connecting the cavity with the lateral edges and the radial cracks at the cavity of the wider stripe in Fig. 7b are very similar to those found in experiments (see Fig. 4f). According to the findings of Martin et al. [9], the enhancement of inter-particle friction also led to an increase of pore formation distant from the void. This is most likely due to very localized assembly heterogeneities on the particle scale, which are always present in the amorphous green samples for DEM calculations.

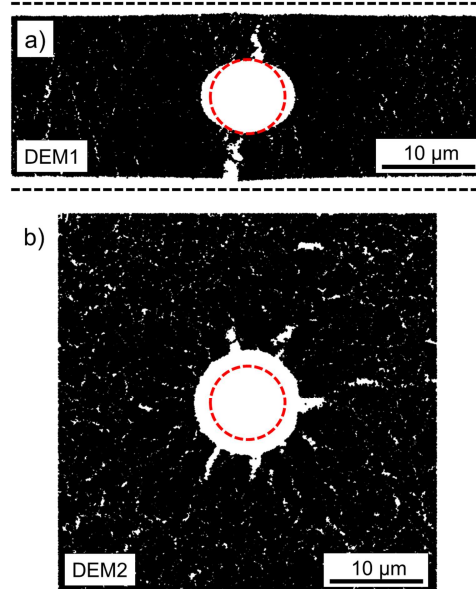


Figure 7: Cracks and pores at the cavity region of stripes with different width sintered on rigid substrate with an increased tangential viscosity coefficient of $\eta = 0.25$.

Although tuning the tangential viscosity coefficient led to a somewhat better consistency between experimental and DEM results concerning the final state of the sintered sample, the temporal evolution and the opening shape of the cracks still differ as is shown in Fig. 8 (upper and middle row). Merely increasing the tangential viscosity coefficient, therefore, is unlikely to be sufficient to explain the discrepancy in the general cracking behaviour observed in the last section.

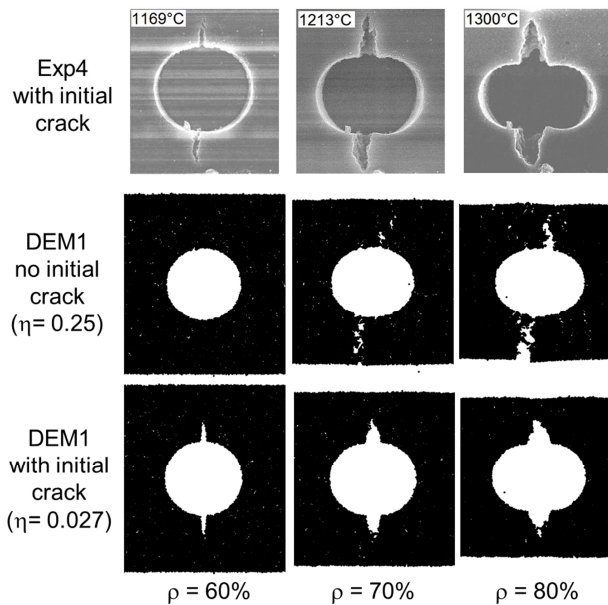


Figure 8: Crack propagation at the cavity region during constrained sintering in the experiment (top) as well as in the DEM simulations without (centre) and with (bottom) predefined initial cracks.

To investigate this discrepancy in more detail, SEM images of narrow experimental stripes taken at the beginning of the sintering cycle had been looked at. These results revealed that very thin micro cracks had already been formed at the cavity at temperatures of just above 1000 °C (i.e. below the onset of free sintering of TM-DAR alumina), which are – likewise to the rupture cracks observed in the final stripe – oriented to the lateral edge. The existence of such hair-line cracks in unsintered thin films has already been observed by other authors [2,6] and might be due to the preceding drying procedure in uncontrolled atmosphere. Since as-dried crack-free films are

expected to be under residual stress, a small additional stress build-up, e. g. due to a thermal expansion mismatch between substrate and film, may be sufficient to induce the formation of such pre-sintering cracks. In addition, the debinding process can also contribute to the development of initial cracks.

Micro cracks similar to the ones found in the experiments were introduced in the DEM simulation by removing thin slides of particles in the corresponding regions similar to the removal of particles for the cavity introduction. This leads to a much better accordance of the final result concerning crack opening behaviour even for simulations with a tangential viscosity coefficient of $\eta = 0.027$ as Fig. 8 (bottom) shows for the DEM1 sample (last row). Both the crack opening and the shape of the propagating crack can be reproduced very well when considering this additional feature. This indicates that pre-sintering micro fractures are a crucial cause for the formation of cracks, which evolve at the cavity during sintering of thin films on a rigid substrate.

5. Summary

The sintering of thin films with pre-defined cylindrical cavities on a rigid substrate has been investigated with a special focus on crack formation at the cavity surface. Contrary to former studies about the evolution of intentionally introduced defects, stresses arising during sintering were studied by FEM calculations and DEM results concerning crack formation were contrasted directly with accompanying experiments on samples with comparable geometrical features. Thus, on the one hand we were able to show that a thorough stress analysis has the ability to predict location, direction and extension of emerging cracks. On the other hand, DEM as a particle-based method turned out to be generally well suited for simulating the experimentally observed crack formation in a natural way without a phenomenological damage initiation criterion. Comparing the results with experiments, however, revealed that the tangential viscosity

coefficient defining the relative sliding behaviour of two particles has to be chosen carefully and prior knowledge about hair-line fractures in the green sample has to be available in order to get a proper match.

Two different stress and crack patterns have been found in this study: Continuous films have a uniform tensile stress distribution around the cavity rim, whereas tensile stresses only occur in a zone between the cavity and the lateral stripe edge in the case of narrow stripe samples. This leads in the first case to cracks forming all around the cavity rim and propagating radially. In the second case, cracks form with their origin at those points of the cavity rim that are closest to the lateral edge that propagate with direction to this edge. Dependent on the stripe thickness, such oriented cracks can expand through the whole sample, i.e. from the cavity to the edge.

For the purpose of avoiding crack formation at predefined vias during constrained sintering of thin films, following actions on geometrical design and manufacturing procedure can be taken according to the results of this study: Unless being in conflict with other conditions for functionality or fitting accuracy, it is beneficial to produce films of low thickness and with clearly defined (i.e. with no sharp edges) voids of large diameter. In addition, it is advantageous to decrease inter-particle friction to the lowest possible level (e.g. by choosing a spheroidal powder with smooth particle surface, leading to a low surface area) in order to promote particle rearrangement, which consequently leads to local stress relief. Moreover, the example of comparing DEM results and experiments concerning crack opening behaviour in Fig. 8 showed that it is crucial to avoid fracture initiation already in the manufacturing steps preceding sintering since hair-line cracks do not heal but can act as a seed for crack opening especially in situations where tensile stresses prevail.

Acknowledgment

This work was supported by the Deutsche Forschungsgemeinschaft (DFG) [grant numbers KR 1729/10-2, GU 993/2-2].

References

- [1] K. A. Peterson, K. D. Patel, C. K. Ho, S. B. Rohde, C. D. Nordquist, C. A. Walker, B. D. Wroblewski, and M. Okandan, "Novel microsystem applications with new techniques in low-temperature co-fired ceramics," *Int. J. Appl. Ceram. Tec.*, **2** [5] 345-363 (2005).
- [2] F. F. Lange, "Densification of powder rings constrained by dense cylindrical cores," *Acta Metall.*, **37** [2] 697-704 (1989).
- [3] F. F. Lange and M. Metcalf, "Processing-Related Fracture Origins: II, Agglomerate Motion and Cracklike Internal Surfaces Caused by Differential Sintering," *J. Am. Ceram. Soc.*, **66** [8] 398-406 (1983).
- [4] D. J. Green, O. Guillon, and J. Rödel, "Constrained sintering: A delicate balance of scales," *J. Eur. Ceram. Soc.*, **28** [7] 1451-1466 (2008).
- [5] R. K. Bordia and A. Jagota, "Crack Growth and Damage in Constrained Sintering Films," *J. Am. Ceram. Soc.*, **76** [10] 2475-2485 (1993).
- [6] X. Wang, Z. Chen, and A. Atkinson, "Crack formation in ceramic films used in solid oxide fuel cells," *J. Eur. Ceram. Soc.*, **33** [13] 2539-2547 (2013).
- [7] F. Li, J. Pan, and A. Cocks, "A new numerical scheme for computer simulation of multiple cracking in ceramic films during constrained sintering," *Model. Simul. Mater. Sc.*, **20** [3] 035008 (2012).
- [8] B. Henrich, A. Wonisch, T. Kraft, M. Moseler, and H. Riedel, "Simulations of the Influence of Rearrangement During Sintering," *Acta Mater.*, **55** 753-762 (2007).

- [9] C. L. Martin, H. Camacho-Montes, L. Olmos, D. Bouvard, and R. K. Bordia, "Evolution of Defects During Sintering: Discrete Element Simulations," *J. Am. Ceram. Soc.*, **92** [7] 1435-1441 (2009).
- [10] T. Kraft and H. Riedel, "Numerical Simulation of Solid State Sintering - Model and Application," *J. Eur. Ceram. Soc.*, **24** 345-361 (2004).
- [11] I. Schmidt and T. Kraft, "Simulation of the co-sintering of composite structures," *Int. J. Mater. Res.*, **101** 933-941 (2010).
- [12] O. Guillon, C. Jamin, and R. K. Bordia, "Effect of drying conditions on patterned ceramic films processed by soft micromolding," *J. Ceram. Soc. Jap.*, **118** [4] 321-325 (2010).
- [13] C. Jamin, T. Rasp, T. Kraft, and O. Guillon, "Constrained Sintering of Alumina Stripe Patterns on Rigid Substrates: Effect of Stripe Geometry," *J. Eur. Ceram. Soc.*, **33** [15-16] 3221-3230 (2013).
- [14] J. Svoboda, H. Riedel, and H. Zipse, "Equilibrium pore surfaces, sintering stresses and constitutive equations for the intermediate and late stages of sintering- I. Computation of equilibrium surfaces," *Acta Metall.*, **42** 435-443 (1994).
- [15] H. Riedel, H. Zipse, and J. Svoboda, "Equilibrium Pore Surfaces, Sintering Stresses and Constitutive-Equations for the Intermediate and Late Stages of Sintering - II. Diffusional Densification and Creep," *Acta Metall.*, **42** 445-452 (1994).
- [16] T. Rasp, C. Jamin, A. Wonisch, T. Kraft, and O. Guillon, "Shape Distortion and Delamination During Constrained Sintering of Ceramic Stripes: Discrete Element Simulations and Experiments," *J. Am. Ceram. Soc.*, **95** [2] 586-592 (2012).
- [17] A. Wonisch, T. Kraft, M. Moseler, and H. Riedel, "Effect of the Particle Size Distribution on Solid-State Sintering: A Microscopic Simulation Approach," *J. Am. Ceram. Soc.*, **92** [7] 1428-1434 (2009).
- [18] A. Wonisch, O. Guillon, T. Kraft, M. Moseler, and H. Riedel, "Stress-Induced Anisotropy of Sintering Alumina: Discrete Element Modelling and Experiments," *Acta Mater.*, **55** 5187-5199 (2007).

- [19] C. Jamin, T. Rasp, T. Kraft, and O. Guillon, "Constrained Sintering of Alumina Stripes on Rigid Substrates: Effect of Substrate Roughness and Coating," *J. Am. Ceram. Soc.*, **98** [12] 3988-3995 (2015).
- [20] T. Rasp, "Modellierung von Anisotropieentwicklung und Rissausbreitung beim Sintern dünner keramischer Schichten (Modelling of anisotropy development and crack evolution during sintering of thin ceramic films)"; PhD Thesis, Karlsruhe Institute of Technology, Karlsruhe, Germany, October 2015.
- [21] S. Timoshenko, and J. N. Goodier, Theory of elasticity; pp. 78-85. McGraw-Hill, New York, 1951.
- [22] C. Hillman, Z. Suo, and F. F. Lange, "Cracking of Laminates Subjected to Biaxial Tensile Stresses," *J. Am. Ceram. Soc.*, **79** [8] 2127-2133 (1996).
- [23] C. E. Inglis, "Stresses in a plate due to the presence of cracks and sharp corners," *Trans. Naval Architect.*, **55** 219-242 (1913).
- [24] S. Martin et al., "Validation of DEM modelling of sintering using an in situ X-ray microtomography analysis of the sintering of NaCl powder," *Comp. Part. Mech.*, **3** 525–532 (2016).
- [25] R. Besler, M. R. da Silva, M. Dosta, S. Heinrich, and R. Janssen, "Discrete element simulation of metal ceramic composite materials with varying metal content," *J. Eur. Ceram. Soc.*, **36** [9] 2245–2253 (2016).
- [26] Z. Yan, C.L. Martin, O. Guillon, D. Bouvard, and C.S. Lee, "Microstructure evolution during the co-sintering of Ni/BaTiO₃ multilayer ceramic capacitors modeled by discrete element simulations," *J. Eur. Ceram. Soc.*, **34** 3167–3179 (2014).